FR 8001271

INIS 1

5. Workshop on laser interaction with matter.
University of Rochester, N.Y, November 5 - 9, 1979.
CEA - CONF 5057

FAST ELECTRON PREHEATING IN EXPLODING PUSHER EXPERIMENTS

C. Bayer, D. Billon, M. Decroisette, D. Juraszek,
D. Lambert, J. Launspach, M. Louis-Jacquet,
J.L. Rocchiccioli, D. Schirmann

Commissariat à l'Energie Atomique, Centre d'Etudes de
Limeil, B.P. N° 27, 94190 - Villeneuve-Saint-Georges-FRANCE

INTRODUCTION

Microballoon implosion experiments in the explosive pusher regime have been performed at CEL with the eight beams glass laser system Octal.

Irradiations have been performed at laser irradiances of a few 10^{15} $W.cm^{-2}$ in 50 ps. Numerous theoretical[1] and experimental works[2] show that in such conditions, laser absorption occurs at critical density in a high density gradient, mainly through resonant absorption, while energy transport processes imply fast electron occurrence and great thermal flux reduction. In a first part of this paper we present an experimental study about the effect of a prepulse in the contrast ratio range 10^{+4} - 10^{+6}. Evolutions of specific absorbed energy, neutron yield, spatial profiles of Silicon resonance lines, ion distribution functions and X-ray pinhole pictures are described and tentatively connected to fast electron occurence.

In flat layered targets irradiation experiments[3] a strong reduction factor of the thermal conductivity of (10^{-2} 10^{-3}) and a fast electrons preheating ratio of 10% have been deduced with respect to the incident energy. Here suprathermal preheat has been diagnosed by X-ray shadowgraphy.This diagnostic is of a particular value in ablatively driven laser implosions [4,5,6]. But for exploding pusher targets, X ray probing in the keV range provided quite useful informations about electron energy deposition in the shell. The backlighter was a Cu-Zn target irradiated by a ninth chain (1 J ; 50 ps). The timing of the probing pulse has been checked using an X-ray streak camera. Time integrated transmission has been interpreted in terms of glass shell heating versus laser intensity.

1. EXPERIMENTAL CONDITIONS

Experiments have been performed with the (8+1) beams Nd laser facility Octal, operated in short pulse regime (50 ps) ; the eight beams delivered typically 40J on target, the ninth one (1 J) being used for diagnostic purposes such as X-ray backlighting.

Target irradiation is performed in cubic geometry (fig. 1) in order to get isotropic energy deposition and beams are focused by f/2 aspherical lenses. More than sixty recording points are currently activated in the target chamber (fig.2) among which thirty two pyroelectric calorimeters (2) and twelve faraday cups (3) for energy balance and control of fast ions occurrence ; X ray pinhole cameras (4) for implosion symmetry and compression evaluation ; X-ray streak camera (5) for compression timing, X-ray plane crystal spectrographs (6) for electron temperature evaluation, T.O.F. magnetic-deflexion spectrometer (7) for alpha particules detection, and at last BF_3 detectors, activated silver counters and scintillator-photomultipliers devices for neutron measurements. Correct beam alignment on target was controlled after each laser shot by 2 ω_o time integrated pictures with a magnitude of 200 (fig. 3).

High energy contrast ratio on target was obtained by inserting a dye cell on each beam of Octal. Randomly occurring prepulses between 0.5 - 3 ns before the main pulse were measured in the power range 1-100 MW (fig. 4).

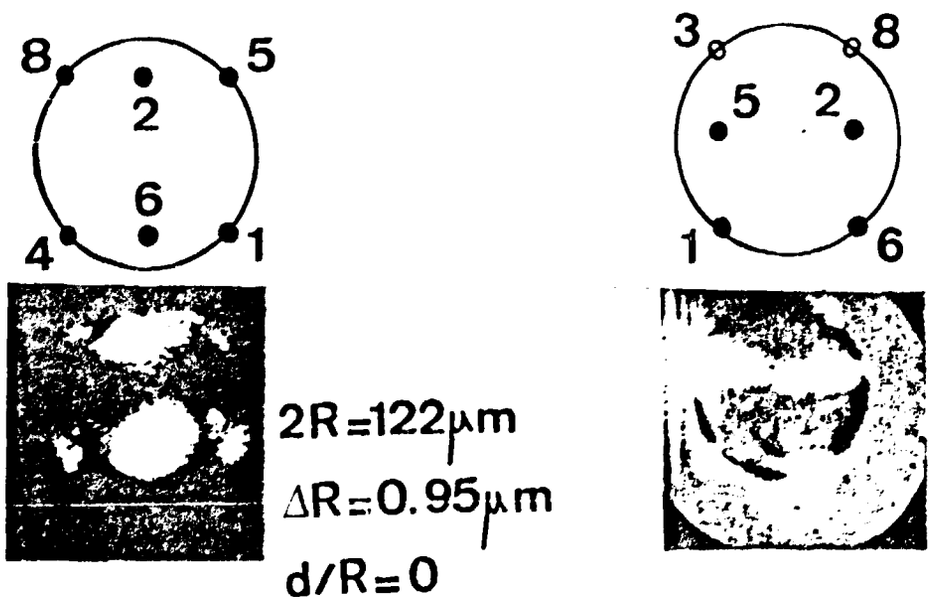

fig.3 : 2 ω_0 time integrated pictures (without prepulse)

Fig 1 : Octal and Camelia implantation

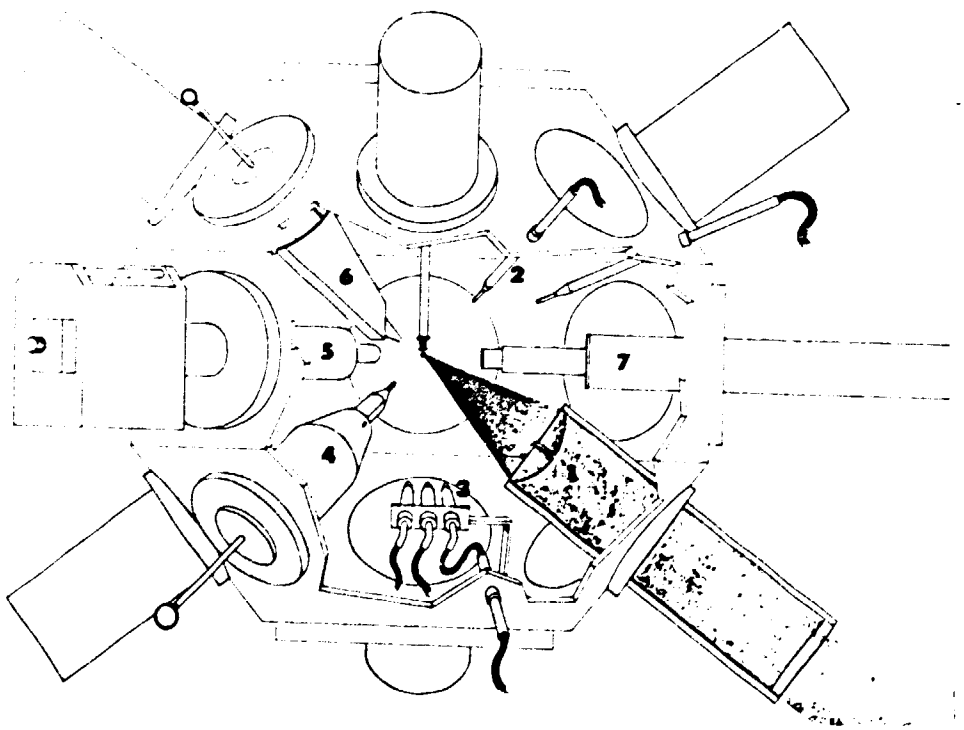

Fig 2 : Camelia chamber with diagnostics implantation

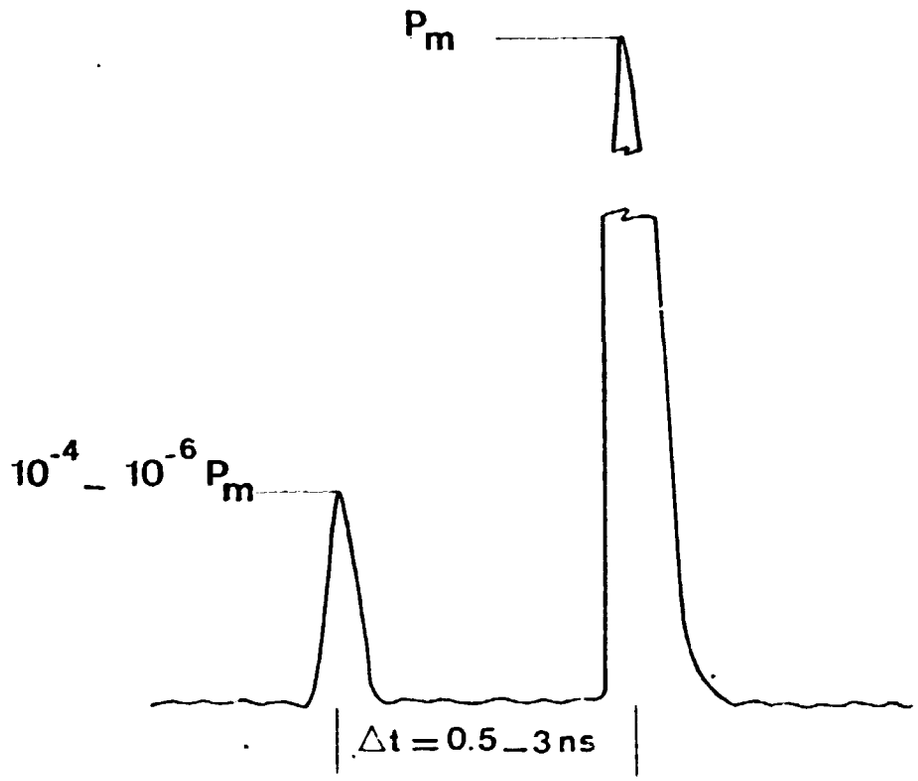

Fig. 4 : Schematic temporal evolution of laser prepulse and pulse powers.

2. TYPICAL RESULTS AND PREPULSE EFFECTS

Imploded targets were glass microballoons typically 80 µm in diameter and 0.68 µm in wall thickness ; however for preheating studies, variations on diameter and wall thickness (by p-xylene coating)were performed.

Results will be presented with the mention "without" or "with prepulse" respectively standing for $\simeq 10^{+6}$ or $< 10^{+4}$ power contrast ratios.

2.1. Energy balance

Results on energy balance are summarized in table I and II, and reported versus incident laser flux in fig. 5. For a high contrast ratio ($\simeq 10^6$) in the incident laser flux range $2.8\ 10^{15}$ - $4.2\ 10^{15}$ $W.cm^{-2}$, the mean absorbed specific energy increases from 0.15 to 0.21 J/mg, variations being fitted by (E_a/M) J/mg $\simeq$ $5.10^{-17}\ \phi_i$ $(W.cm^{-2})$. In table I, (R + T) stands for non absorbed energy measured in the focusing lens cones, including refraction and scattering (R) and transmission (T), T having been evaluated

in one beam irradiation, (r) stands for refracted and scattered energy, measured in the target chamber outside of the lens cones and (A) the overal absorption coefficient.(A) was evaluated within

Table I

P_{GW}		650	950
ϕ_i	$W.cm^{-2}$	$2.8.10^{15}$	$4.2.10^{15}$
R + T	%	23.5	24
r	%	60.5	61.5
A	%	16	14.5
$\frac{E_a}{M}$	J/ng	0.15	0.21

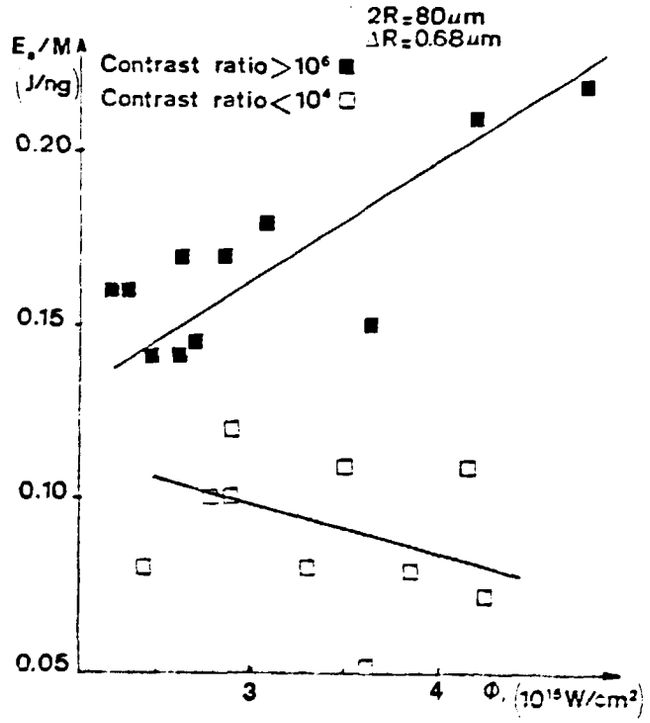

Fig. 5 : Mean absorbed specific energy versus incident laser flux with and without prepulse

the assumptions of refraction and scattering isotropy which seem valid since fluctuations of calorimeters signals

$$\Delta\left(\frac{dE_r}{d\Omega}\right) \Big/ \left\langle\left(\frac{dE_r}{d\Omega}\right)\right\rangle \simeq 0.24$$

were close to those of incident energy $\frac{\Delta E_i}{\langle E_i \rangle} = 0.2$

In the case of a prepulse of relative intensity 10^{-4} (table II) the absorption is about 50 % lower due to an increase of refraction and scattering. This results in a mean absorbed specific energy slightly decreasing around 0.1 J/ng.

Table II

P_{GW}		650	950
R + T	%	25	27
r	%	64	66
A	%	11	7
$\frac{E_a}{\bar{M}}$	J/ng	0.1	0.08

These results suggest that the prepulse drives an early hydrodynamical flow carrying the critical density away from the initial target surface, with a smooth density gradient. This leads first to a lowering of the interacting flux for the main pulse and thus a lowering of the resonant absorption contribution[7] ; moreover, a larger subcritical plasma enhances non linear processes such as stimulated Brillouin scattering[8].

2.2. Ion distribution functions analysis

Ion distribution functions are reported in fig. 6. They have been deduced from time of flight measurements with faraday cups. Isotropy of plasma expansion could be deduced from signals identity within a few percent. But it appeared strong features modification according to the prepulse level.

In the case of a high contrast ratio (10^6) the velocity spectrum obtained with $\bar{Z} = 10$ and $\bar{M} = 20$ presents a high velocity component for $v > 10^8 cm.s^{-1}$. In fact, the distribution function can be fitted by adding three maxwellian distributions (as indicated in the cartoon) characterized by a mean velocity respectively 10^7 $cm.s^{-1}$, $2.5\ 10^7$ $cm.s^{-1}$ and $1.8\ 10^8$ $cm.s^{-1}$.

The second one, we shall call "thermal" seems to be attributed to corona ions directly expanding outwards from the target. The "cold" first one may be due to ions initially propelled inwards the target, and expanding off the core after stagnation. The third one

is a hot distribution which may be interpreted composed of fast ions driven by suprathermal electrons coming from resonant absorption.

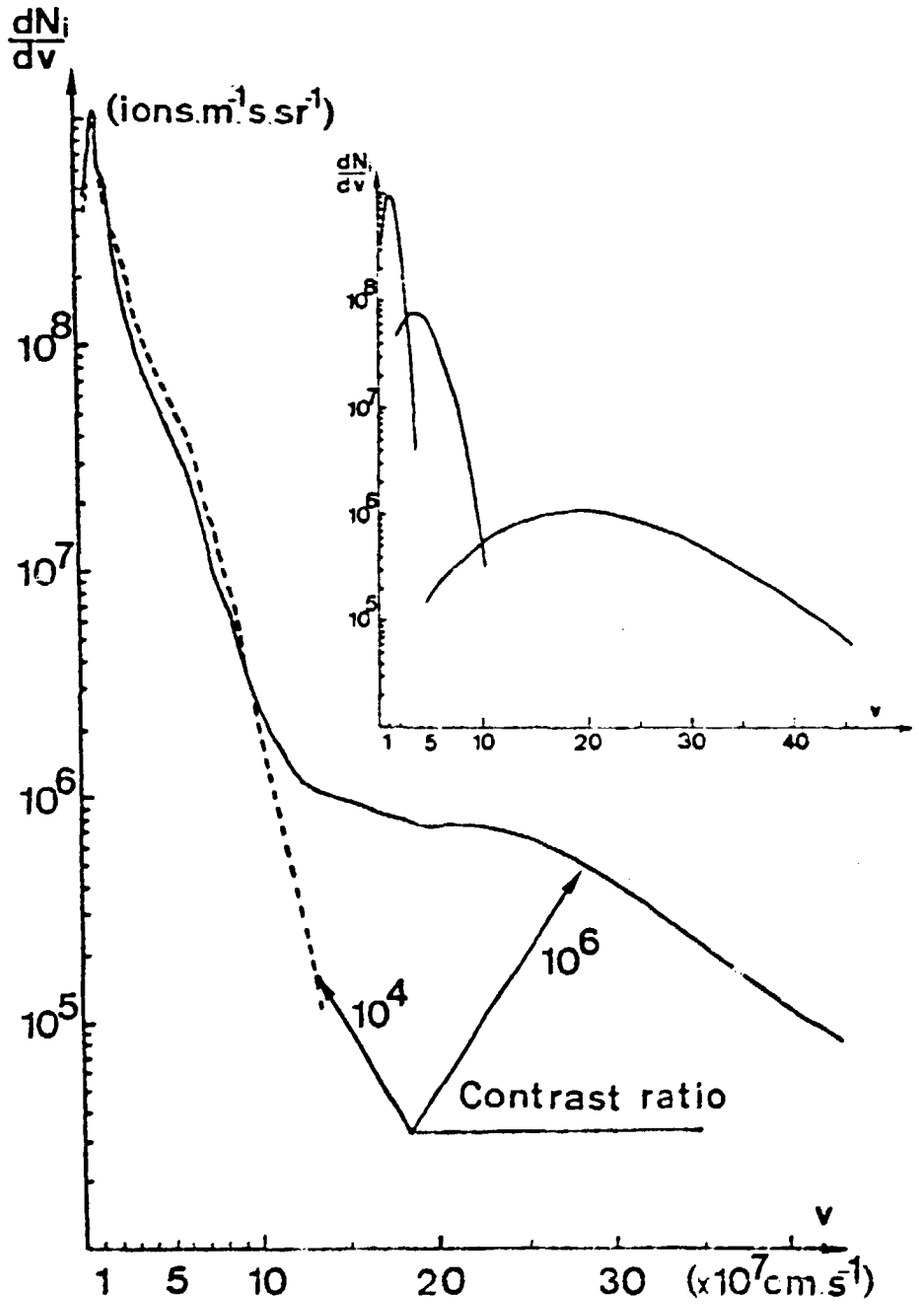

Fig. 6 : Ions velocity spectrum with and without prepulse ; the cartoon represents maxwellian distributions modelisation

In this special case, the ion kinetic energy for velocities greater than $10^8 cm.s^{-1}$ corresponds to 50% of the total absorbed energy, the "cold" and "thermal" distributions carrying respectively 12% and 28% of the total ion kinetic energy, and 78% and 20% of the total mass.

In the case of a prepulse (10^4 contrast) the "hot" distribution has quite disappeared (the proportion of energy carried away by ions velocities $> 10^8$ cm.s^{-1} being less than 5%) while the cold and thermal distribution account for respectively $\simeq$ 20% and $\simeq$ 80% of the kinetic energy. Desappearence of fast ions is difficult to connect unambignously to fast electron desappearence, as the early plasma set up by the prepulse may cause ions slowering down. However, masses carried out by the thermal distributions in shots with high and low contrast ratio correspond respectively to a glass ablated thickness of 0.14 µm and 0.15 µm, inferring that a thickness $<<$ 0.15 µm has been ablated by the prepulse. In the pessimistic assumption that 0.1 µm were ablated by the prepulse, calculation in spherical geometry of stopping power of Si^{14+} ions in SiO_2 absorbing material at different temperatures and densities, have been performed, taking into account electron collision (Bohr formulation) and nuclear collision (Bethe formulation). Table III presents the cut-off speed V_c such that ions whose velocities are greater than V_c, are not stopped by the ablated material. It can be seen that in every case V_c is lower than $10^8 cm.s^{-1}$

TABLE III

n_e \ absorbing material	$Si O_2$ Cold	$Si O_2$ 1 keV
$7.5\ 10^{23}$ ($\rho = \rho_o$)	$1.2\ 10^8$ cm/s	-
10^{21}	$9\ 10^7$	$8.8\ 10^7$
10^{20}	$6\ 10^7$	$5.2\ 10^7$
10^{19}	$3.5\ 10^7$	$3.8\ 10^7$

Thus fast ions disappearance seems to be related to a strong reduction in fast electron generation due to an important decrease in resonant absorption.

2.3. Neutron emission

Neutron yield for standard microballoons with 10-30 bar DT pressures was typically 10^6 - 10^7 in the absorbed specific energy range 0.1- 0.3 J/ng and a high contrast ratio. However it decreased of nearly one order of magnitude in the case of a prepulse. Similar results are described in ref.9.

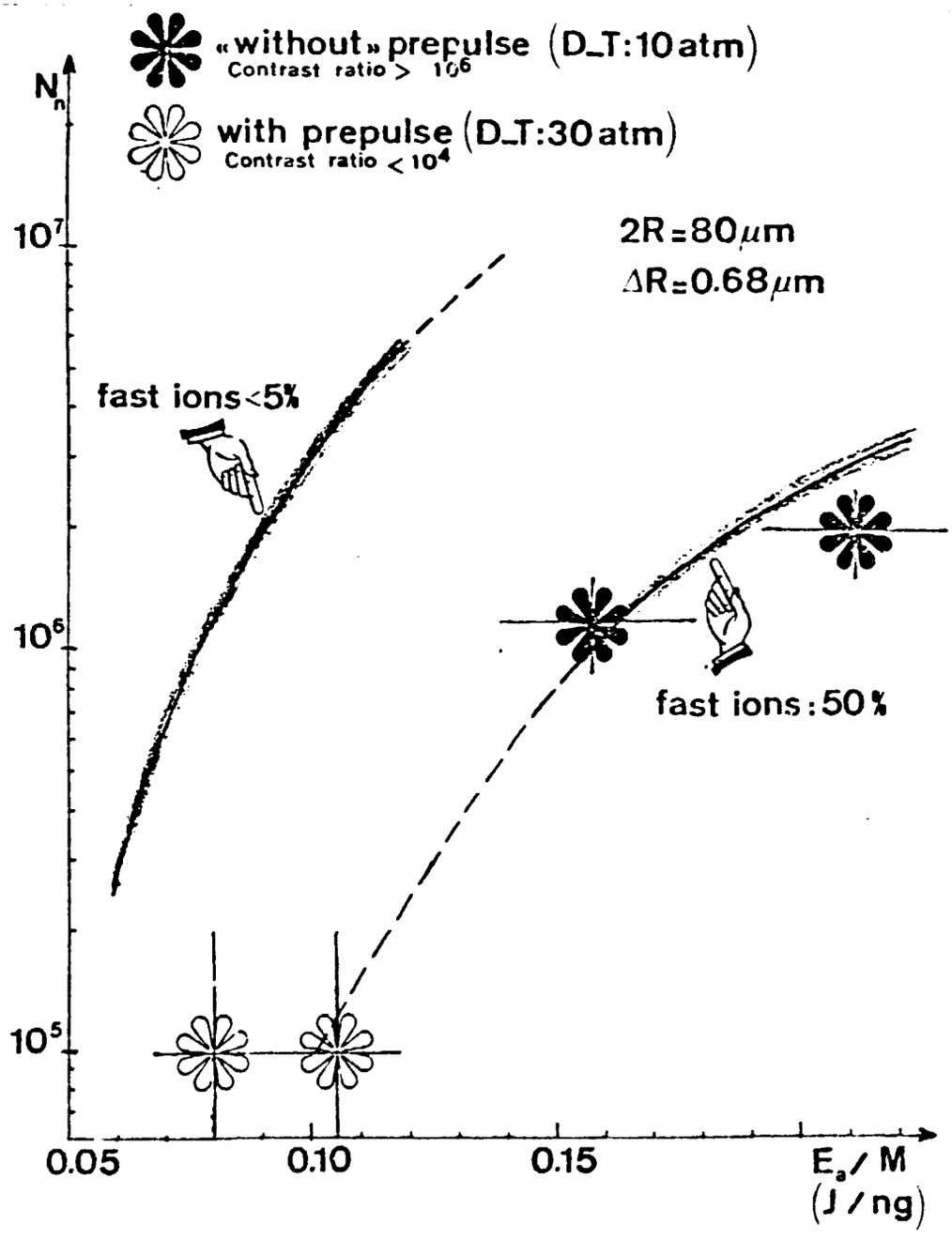

Fig. 7 : Experimental neutron yields versus mean absorbed specific energy, compared with theoritical model, with and without prepulse.

In fig. 7, experimental results have been compared to numerical evaluations performed using the analytical model of[2]. Two theoretical curves have been drawn for fast ion energy percentages 5 % and 50 % in view to fit with experimental observations with and without prepulse. High contrast ratio results appear in good agreement with the model, but low contrast ones are much below the related previsions. In fact, as all results correspond to the similar useful absorbed specific energy (as defined in[2]) this can signify that low contrast ratio results cannot be compared to the explosive pusher regime.

2.4. X-ray spectroscopy

In the followings, the word "core" will stand for the compressed zone, including both glass and D.T.

Prepulse consequenses were also seekeed for by X ray analysis in the 4 to 8 Å range, with spatial resolution about 10 µm. One dozen shots have been selected for this presentation, ported into two flux ranges series 800 - 850 GW and 950 - 1100 GW.

Emitted line power integration (table IV)

For helium-like Silicon α and β transitions, as for hydrogen-like Lyman α, no internal spectral resolution was possible, due to instrumental width exceeding Stark width. However, satellite-lines can be distinguished from resonance ones. Theoretical interest from introducing these satellites in line power ratios is low but it allows verification that their unwanted contribution would not qualitatively change any result. Satellites included figures are in brackets

Table IV

	lines energy ratios	
	with prepulse (A)	Without prepulse (S)
Low flux 800-850 GW	$\frac{H_\alpha}{He\alpha}$ = 0·27 (0.20)	$\frac{H_\alpha}{He\alpha}$ = 0.75 (0.62)
	$\frac{He\beta}{He\alpha}$ = 0·34 (0·18)	$\frac{He\beta}{He\alpha}$ = 0·58 (0·35)
High flux 950-1100 GW	$\frac{H_\alpha}{He\alpha}$ = 0·21 (0.12)	$\frac{H_\alpha}{He\alpha}$ = 0.47 (0.35)
	$\frac{He\beta}{He\alpha}$ = 0.11 (0.10)	$\frac{He\beta}{He\alpha}$ = 0.65 (0.39)

Core dimensions

Spatial analysis of the spectrograph films shows that for Helium like lines there is no distinction between core and corona emissions and the spatial line shape is a mere trapezium.

But for hydrogen-like Hα, the core emission may be figured as narrow trapezium superposed upon a wide one, representing corona emission.

The core diameter measured from trapezium basis is

With prepulse $\langle 2\ Ko \rangle_A = 17\ \mu$

$\langle 2\ Ro \rangle_S = 23\ \mu$

(A stands for with prepulse ; S for without prepulse)

This shows a 35 % decrease of diameter and it cannot be an artefact since, when omitting the extreme values into the averaging, the difference keeps higher than 25 %.

Interpretation of such facts can lie in :
- either the acceptance of better compression because of prepulse
- either the fact of a lower core-temperature with prepulse (that could agree with a lesser neutron production)
- either the fact that the prepulse partly breaks the microballoon letting it leak during compression (that could be demonstrated by a heavy gaz doping of D.T, Ne for example)

Corona dimensions

Since plasma-requirements for H-like and He-like emissions are not exactly the same, measurements of corona diameter from these two kinds of lines do not exactly coïncide (apparent diameter from H-like analysis being narrower), but the ratio of figures with and without prepulse is quite the same in both cases.

We find by Heα analysis

With prepulse $\langle 2\ R \rangle_A$ = 230µm dispersion less than 10 %

Without prepulse $\langle 2\ R \rangle_S$ = 190µm dispersion less than 12 %

So the corona is 20 % larger after a prepulse.

If we admit that the difference between H-like and He-like emission borders is representative of the density gradient scale length, we find it 20 % larger with prepulse.

By Hα analysis, we see no diameter difference between "with" and "without" cases exceeding experimental resolution ; we measure a main diameter very similar to the original microballoon'one, as by pinholes cameras. Such a concordance between H-like spectrograph result and pinhole results but contradiction with He-like ones is not worrying since He and continous emissions require very similar conditions.

For He-like emission, density and temperature requirements are so different that, although we cannot distinguish temporaly different phenomena, we can state that the emissing matter elements are different, and confused only because of time integration.

So we can use different criteria for measuring H-like and He-like emissions diameters. The He-like figures listed above correspond to measurements of diameter between the intersections of zero-level with the two straight tangential lines to the spatial profile at half profile width and altitude

Spectral lines lumination

The values listed above integrate the total emission seen from a planar window

- materially limited in one direction by the hedges of slit
- virtually limited in the orthogonal direction by the cristal diffraction width and the dimension of plasma emitting zone itself.

Each position in the spatial analysis direction is then an image from a section of the plasma by a plane originated from the spectrograph slit.

Different values of these plane widths correspond to different values of λ, thus preventing us from determining a direct diagnostic from measured $\frac{H\alpha}{He\alpha}$ and $\frac{He\beta}{He\alpha}$ ratios, although their real knowledge would enable us to determine Te and Ne by the use of a suitable model.

So we must use only

$$\frac{\left(\frac{He\ \beta}{He\ \alpha}\right)_A}{\left(\frac{He\ \beta}{He\ \alpha}\right)_S} \quad \text{and} \quad \frac{\left(\frac{H\alpha}{He\alpha}\right)_A}{\left(\frac{H\ \alpha}{He\ \alpha}\right)_S}$$

Coronal temperatures

According to the model

$$\frac{\left(\frac{He\beta}{He\alpha}\right)_A}{\left(\frac{He\beta}{He\alpha}\right)_S} = \frac{e^{\frac{-1}{kT_A}(h\nu_\beta - h\nu_\alpha)}}{e^{\frac{-1}{kT_S}(h\nu_\beta - h\nu_\alpha)}}$$

The variation range of temperature in the prepulse occuring cases can be evaluated taking account of table IV, from temperatures of without prepulse cases.

We present the results for a fairly excessive range of Ts variation

For lower flux experiments Ts = 500 eV T_A = 270 (235) eV
Ts = 2000 eV T_A = 460 (360) eV

For higher flux experiments Ts = 500 eV T_A = 130 (155) eV
Ts = 2000 eV T_A = 165 (200) eV

Brackets figures are obtained from the ratios including satellites

So, for the coronal zone, prepulses induce a lowering of electron temperature, to be compared to the extending of characteristic density gradient lenght

Compression evaluation

For the core investigation, the problem is there is no distinction possible about which part of helium-like emission is really due to the core-zone.

As the spatial shapes are the same kind of trapezia in both cases with and without prepulse, we may postulate that the ratios of emissions are similar

$$\frac{(He\alpha \text{ core})}{(He\alpha \text{ corona})_S} \sim \frac{(He\alpha \text{ core})}{He\alpha \text{ corona})_A}$$

With the help of this hypothesis we can get an idea of core density. In ETL model, Saha equation implies

$$\frac{H\alpha}{He\alpha} = \frac{A_H}{A_{He}} \cdot \frac{N_H}{N_{He}} = \frac{1}{n_e} \cdot \frac{A_H}{A_{He}} \cdot \frac{e^{-\frac{h\nu_H}{kT}}}{e^{-\frac{h\nu_{He}}{kT}}} c\,(kT)^{3/2} \cdot e^{-\frac{Xi}{kT}}$$

where : Xi are ionization potentials for H_e like silicon and (A_{H_i}, A_{He}) Einstein emission coefficients

So

$$\frac{n_{e_A}}{n_{e_S}} = \frac{\left(\frac{H\alpha}{He\alpha}\right)_S}{\left(\frac{H\alpha}{He\alpha}\right)_A} \; e^{\left(\frac{1}{kT_A} - \frac{1}{kTs}\right) \cdot \tilde{V}} \cdot \left(\frac{Ts}{T_A}\right)^{3/2}$$

Where $\tilde{V} = h\nu_H - h\nu_{He} + Xi$.

Experimentaly, we find

$$\frac{\left(\frac{H\alpha}{He\alpha}\right)_A}{\left(\frac{H\alpha}{He\alpha}\right)_S} \sim 0,4 - 0,3$$

As apparent core compression is higher with than without prepulse, but neutron yeald lower, the use of Saha equation is coherent with

$$T_{A\,core} < T_{S\,core} \qquad \left(\frac{T_A}{T_S}\right)_{core} \sim 0,3$$

$$Ne_{A_{core}} > Ne_{S_{core}} \qquad \left(\frac{Ne_A}{Ne_S}\right)_{core} \sim 10$$

$$T_{S_{core}} > 2 \text{ keV}$$

Lowering of glass compressed temperature seems to be in agreement with a lowering of suprathermal shell preheat, modifying the inner shell pressure profile.

Thus an increase of density may be interpreted as a more ablative regime developped as a consequence of the prepulse effect.

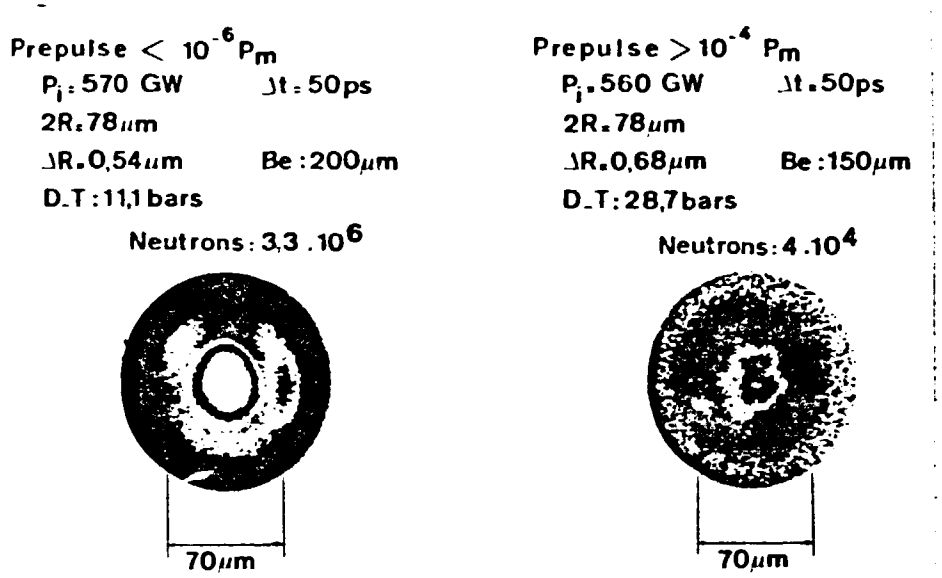

Fig. 8 - X-ray time integrated pin-hole pictures with and without prepulse.

2-5. Volume compression

Volume compression was inferred from X-ray pinhole photographs recording both X ray lines and continuum emission (fig. 8). In high contrast ratio experiments, the core was easily studied, as it looks spherical, with a high emittance compared to corona. Diameter was typically < 20 μm leading to volume compression of the order of 60. In the particular case of figure 8, film saturation prevents us from compressed DT analysis. With a prepulse, the core appears smaller in dimension, less spherical and rather perturbed, with a strongly reduced emittance.

Compression hydrodynamic was also studied in a simple way by coupling an X ray streak camera with a slit parallel to the temporal axis (figure 9). On the film, time delay between corona and core emissions as well as their durations are directly evaluated along the temporal axis, while corresponding dimensions are seen on the spatial axis. For low prepulse experiments, the collapse time can be identified as the time delay between corona and core emission, as both appear well separated, with fast rise time and sharp space gradients. In the case of important prepulse (fig.10) the core/corona contrast is reduced like in fig. 8, core and corona emissions present smoother rise times and space gradients and the collaspe time appears smaller [9]. These results confirm spectroscopic ones as for the smoother density gradients, but the so called collaspe time cannot be compared to the previous, as obviously refering to a strongly different situation

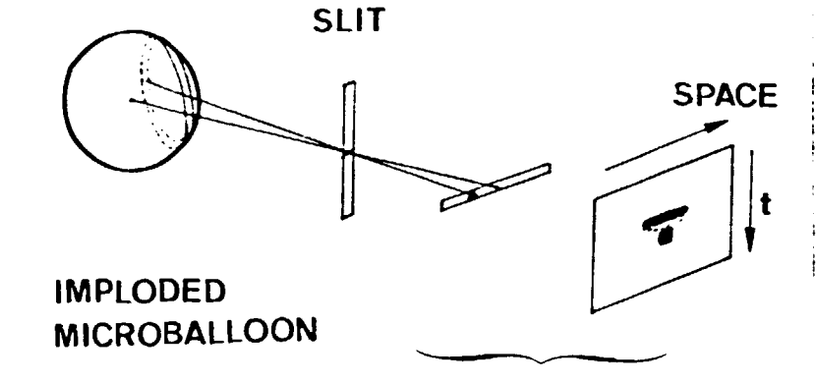

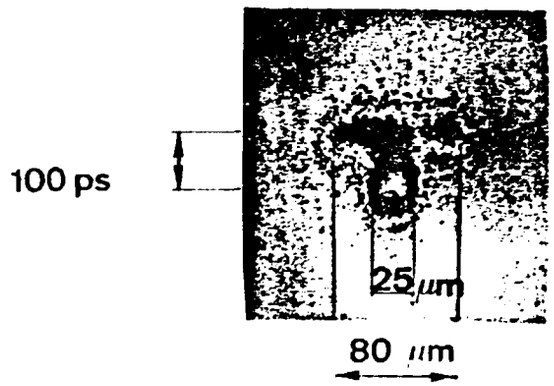

Fig. 9 - Temporally and spatially resolved (in planes) X-ray streak camera recording, without prepulse.

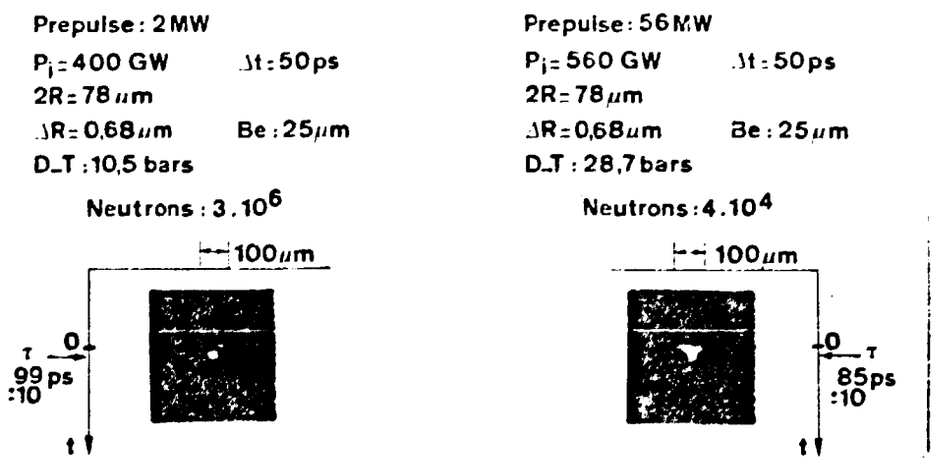

Fig. 10 - X-ray streak camera recordings with and without prepulse

2-6. Conclusion

According to these results, the following phenomenological description of the prepulse effect can be proposed :

The prepulse effect results in an increased critical radius and a smoothered density gradient. The first consequence is a lowering of the irradiation intensity ϕ_i for the main pulse and the development of scattering processes such as stimulated Brillouin scattering, lowering the absorption efficiency. The second effect is a decreased contribution of resonant absorption, both for photon absorption - as an increase of critical radius reduces the angle of incidence of P polarized elementary beams - and for fast electron emission, whose temperature varies as $\phi_i^{0.4}$ [10].

The last point appears as the most important, for the explosive pusher relies on fast electrons shell heating. Indeed fast ions disappearance seems to evidence a lesser suprathermal electron generation. At last, neutrons are no more explained by an explosive pusher analytical model, and arise from a colder and inhomogeneous but probably more compressed core.

All these results give evidence of a regime noticeably different from the explosive pusher. They seem to be related to recent plane targets experiments [3] which have shown in similar conditions (80 ps - 10^{15} W.cm^{-2}-1 µm wall thickness) that a slight flux reduction led to the transition from an explosive situation towards a more ablative one, with a rearwards motion of the whole target.

3 - X-RAY BACKLIGHTING

3-1. In order to test fast electron preheating, an X ray backlighting diagnostic was used. Experimental arrangement consisted of (fig. 11)

- An X-ray source obtained by focusing the ninth beam (1 J ; 50 ps) of the Octal facility, with a f/2 lens (f = 190 mm) on a brass plane target. A 50 to 100 µm diameter plasma was produced emitting a short pulse of soft X rays (≃ 50 ps duration) 1. to 1.5 keV spectral range.

- An X-ray pinhole type camera using two pinholes (15 µm diameter) and a kodirex film. For each shot, we analyse the following images; the X ray source alone providing with the incident X ray backlighting intensity ; the imploded microballoon alone, delivering its own emission which appears as a noise signal in X-ray probing ; at last the source observed through the target, providing us with data on X ray transmitted intensity added to microballoon emission. An example of the three pictures is also shown on the figure 11.

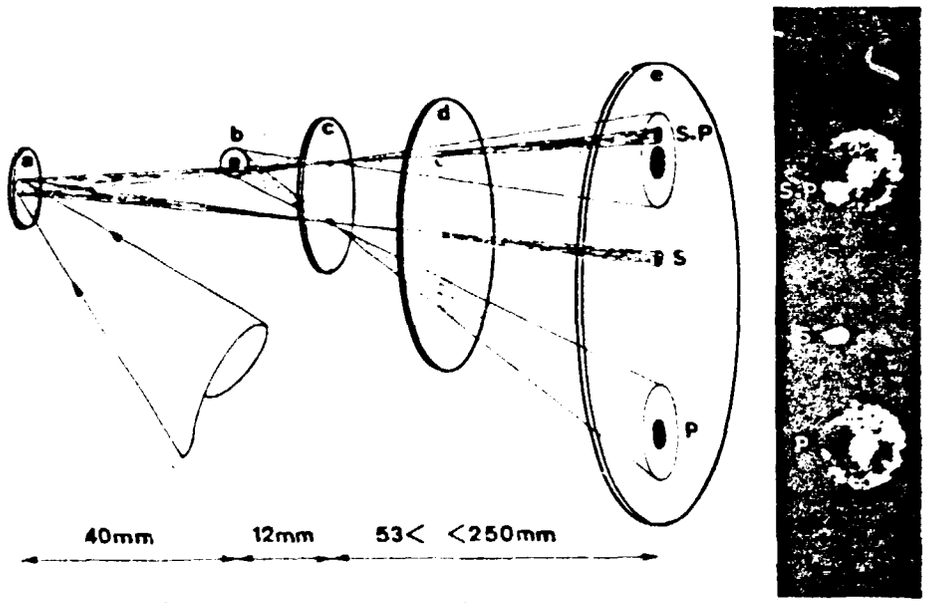

Fig. 11 - Experimental X-ray backlighting arrangement and recording a) X-ray source ; b) imploded microballoon ; c) double pinhole-disc (300 μm separation) ; d) aluminum foil ; e) recording film ; S) image of X ray source alone ; P) image of imploded microballoon alone ; S+P) the source observed through the imploded microballoon

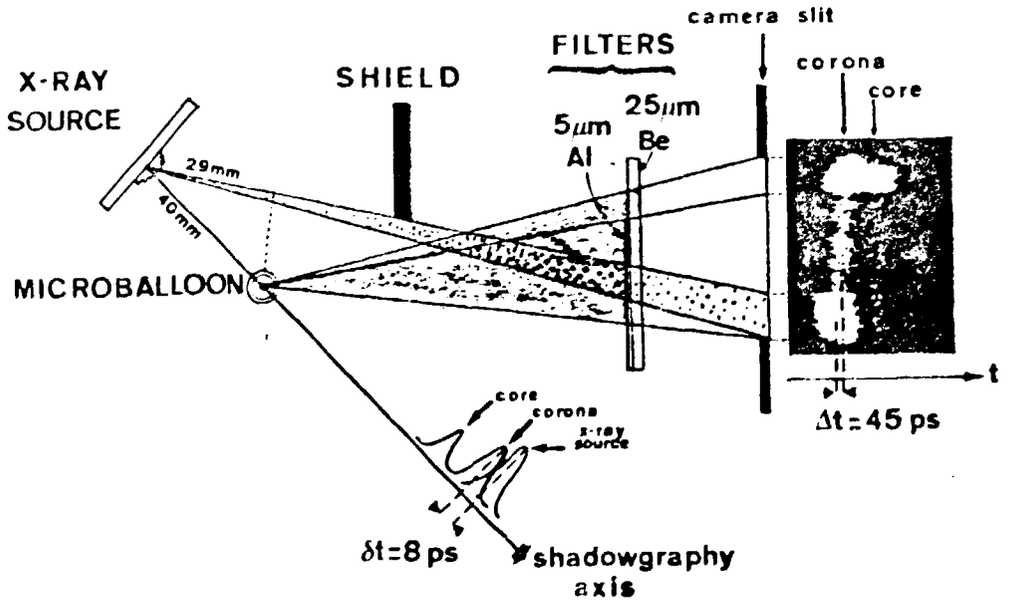

Fig. 12 - Experimental setting for temporal positioning of X-ray source and microballoon emissions.

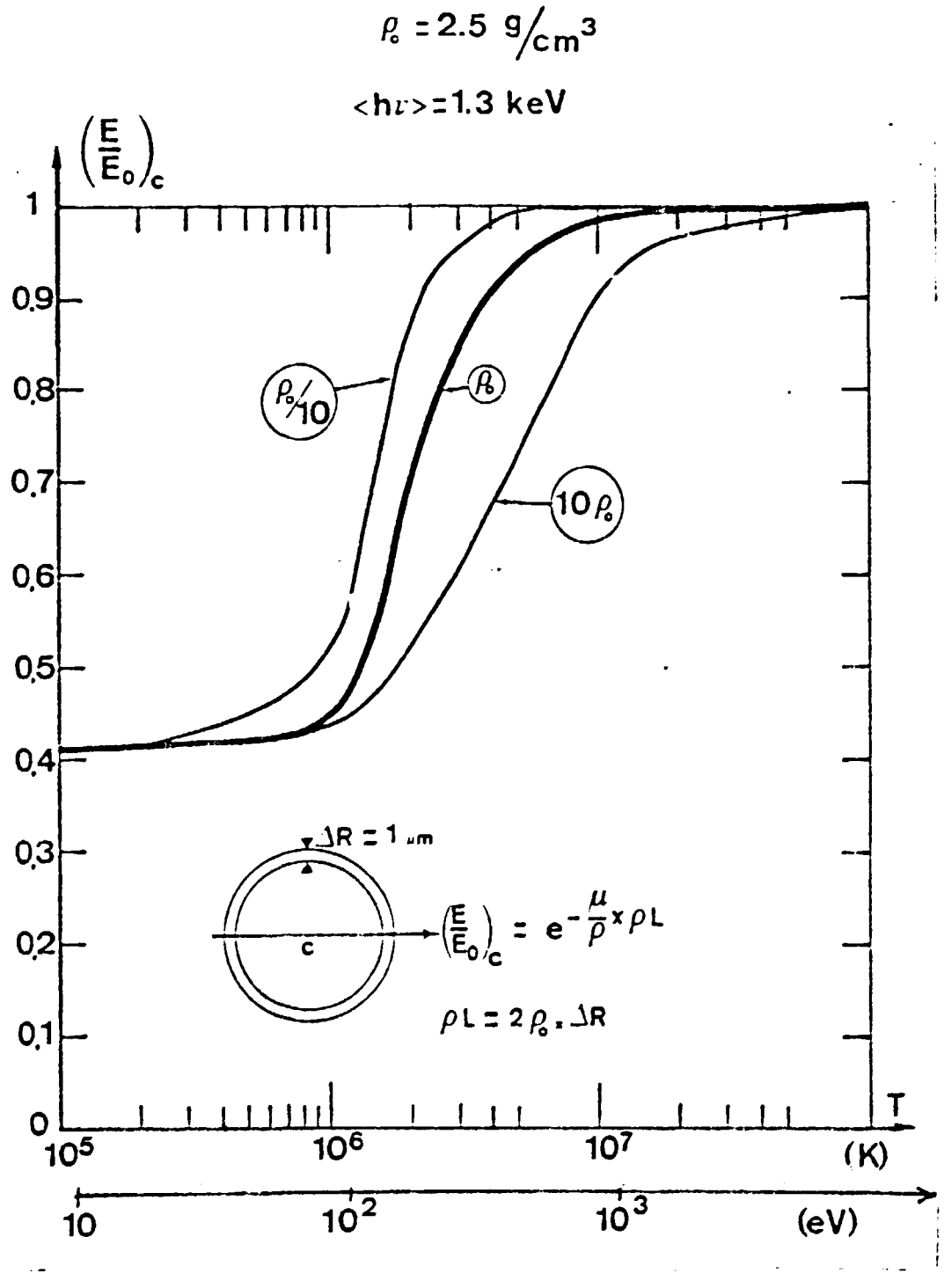

Fig. 13 - Glass microballoon transmission versus temperature.

In order to optimize the signal to noise ratio on the film, X ray source and microballoon emissions were filtered by an aluminium foil (5 to 25 μm thickness). Thus, microballoon emission above 1,56 keV (Al K-edge) was strongly reduced. As an example, with 10 μm Al thickness, transmission is 0,2 at 1.3 keV and 1.7×10^{-3} at 2 keV.

Moreover, the probing axis was slightly shifted from the target center to reduce the influence of the core emission. But transmission measurements E/Eo were normalized for the center (noticed(E/Eo)c) using a simple geometrical assumption of a uniform spherical absorbing shell.

The aim of the experiment was to probe that the shell, although heated by fast electrons,is not yet significantly explosed. The probing time had to be late enough to allow the fast electrons to be generated but it also had to keep previous to the disassembly time occuring during the laser pulse. Practically in the experiment we present here, it was adjusted to about - 10 ps with respect to the maximum of laser pulse by means of an optical delay line inserted on the diagnostic laser beam. It was measured by an X ray streak camera[11] in another direction as shown on figure 12. A shield parthy hid the X ray source emission on the camera slit in order to distinguish both corona and core microballoon emissions and X-ray source emission. Microballoon emissions were filtered by two kinds of filters (25 μm Be alone or 25 μm Be with 5 μm Al) to adjust intensities on the photocathode. Thus, it was verified that duration of X-ray source emission was shorter than implosion time. On the recording shown on figure 12, the delay (Δt = 45 ps) measured between source and corona emissions corresponds to an advance δt = 8 ps of the diagnostic pulse on shadowgraphy axes.

Pratically, a transmission measurement needed three shots :

- The first one with X ray source alone to compare pinholes transmission ;
- the second one with X-ray source through the microballoon not imploded to provide us with a reference of cold glass transmission ;
- the last one with the irradiated microballoon

Figure 13 shows theoretical variations of the transmission at the center $(E/E_o)_c = \exp - 2 \mu \Delta R$, versus temperature, calculated for different densities but with the product $\rho \cdot \Delta R$, kept constant and equal to $2,5 \times 10^{-4}$ g/cm^2 ; μ is the absorption coefficient at $< h\nu >$ = 1,3 keV (corresponding to X ray source) taking into account bound-free, free-free and Compton effects and stimulated

emission. It is the large increase of the transmission above 100 eV (relatively to the cold glass transmission) which made possible an evidence of preheat in this temperature range

Moreover, for T < 100 eV transmission is weakly dependant of density. Consequently, position of probing time with respect to the implosion beginning was not critical, and cold glass transmission was a reference in itself for the study of the wall preheat.

Evolution of $\frac{(E)}{(Eo)C}$ versus the wall thickness is presented on figure 14 fo 80 µm diameter microballoons, similar shots are gathered in rectangles ; a, b, c correspond to about the same incident laser flux (2×10^{15} W/cm^2), d corresponds to 5×10^{14}W/cm^2 All of them have been performed in the high contrast ratio situation.

Experimental values cf cold glass transmission are also reported in good agreement with the theoritical curve exp - 2 µ.ΔR.

By looking at a, b c, cases, transmissions greater than those in the cold glass case were only obtained with thinnest targets and higher flux (a)

Moreover experiments (a) agree well with the model in ref 2 as for the neutron yield versus absorbed specific energy. Thus high transmissions are related to an important fast electron preheat, and are significant of typical explosive pusher regime.

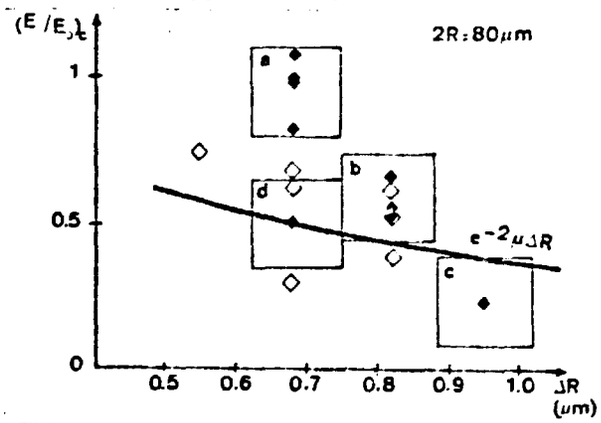

Fig. 14 - Measured transmissions versus wall thickness for 80 µm diameter microballoons ; hollow squares correspond to cold glass whose theoretical transmission is exp(- 2 µΔR) - black squares correspond to microballoons imploded at different fluxes : (2 ± 0.5) 10^{15}W/cm^2 (a, b, c) ; 5.10^{14}W/cm^2 (d). Vertical bars correspond to the maximum experimental dispersion and horizontal bars to the wall thickness uncertainty.

4. Conclusion.

Experimental studies concerning fast electron preheating in exploding pusher type implosion experiments have been performed at the level 1TW with glass microballoons typically 80 µm in diameter and 0.8 µm in wall thickness.

First, effects of a prepulse on energy balance, neutron yield and X-ray emissions were interpreted as the consequence of a lack in fast electrons generation, transferring the implosion in a quite different regime.

Second, fast electron preheating was measured by X-ray backlighting . This diagnostic allows to determine the maximum wall thickness ensuring a microballoon to be implosed in explosive pusher regime.

Authors wish to thank J.C. Courteille, and laser team for OCTAL Management, the target fabrication and data acquisition teams for valuable contribution, and J. Bouard, H. Croso, G. Franzini, J.P.Godefroy, J.Kobus, D. Meynial, J. Turberville, for technical assistance.

REFERENCES

1. E.B. Goldman, J.A. Delettrez and E.J. Thorsos
Nucl. Fus. 19, N° 5, 555 (1979)
2. E.K. Storm et al.
Phys. Rev. Lett. 40 , 1570 (1978)
3. J.C. Couturaud and al. 9th Annual Conference on anomalous absorption of electromagnetic waves (ROCHESTER 1979)
4. J. Launspach and al. Annual meeting of the Am. Phys. Society Nov. 1975, St PETERSBURG Florida
5. M.H. Key et al.
Phys. Rev. Lett. 41 , 1467 (1978)
6. D.T. Attwood
IEEE, Journal of Quantum Electronics Q.E. 14, 909 (1978)
7. J.J. Thomson, C.E. Max, J. Erkkila and J.E. Tull
P.R.L., 37, N° 16, 1052 (1976)
8. D.W. Phillion, W.L. Kruer and V.C. Rupert
Phys. Rev. Lett. 39, N° 24, 1529 (1977)
9. D.T. Attwood, L.W. Coleman, J.E. Swain, D.W. Phillion, K.R. Manes, D.S. Bailey and Y.L. Pan
UCRL 78739 - 10th Conference on Laser Interaction with Matter PALAISEAU, France, Oct. 18/22 1976
10. UCRL 50021 - 76 LLL Laser Program Annual Report (1976)
11. J.P. Gex, N. Fleurot and R. Sauneuf
Rev. de Phys. Appl. 12, 1049 (1977)